An ancient role for conserved innate immunity transcription factors in holobiont self-recognition

Bin Yang*[1], Benedict Yuen*[2], Bernard M Degnan[#] and Sandie M Degnan[#]

Centre for Marine Science and School of the Environment, The University of Queensland, St Lucia 4072 Brisbane Australia

* Contributed equally to this study
[1] Current address: Garvan Institute of Medical Research, Sydney, Australia
[2] Current address: Eco-Evolutionary Interactions Group, Max Planck Institute for Marine Microbiology (MPIMM), Bremen, Germany
[#] Corresponding authors

Abstract

Animal innate immunity may have evolved to regulate host-symbiont interactions using ancient and highly conserved animal transcription factors (TFs). We test this proposition by comparing cellular and transcriptional responses of a marine sponge presented with either native symbiotic or foreign bacteria. In contrast to foreign bacteria, experimentally introduced symbionts are quickly transported across the sponge epithelial boundary to underlying phagocytic amoebocytes. Numerous conserved immunity TFs, including NF-κB, IRF, STAT, AP-1, ETS, SMAD and nuclear receptors, pattern recognition receptors (PRRs) and signaling pathways are simultaneously activated. IRF translocates to the nuclei of amoebocytes that have engulfed the symbionts, followed shortly after by NF-κB, suggesting that both are critical to symbiont recognition. Nuclear localisation of STAT occurs in cells that do not have the symbionts. Foreign bacteria, in contrast, are internalised more slowly and do not induce the nuclear translocation of NF-κB, IRF or STAT, nor do they induce the upregulation of most other immunity genes. Instead, they induce a xenobiotic response. These findings suggest that the shared ancestor of sponges and other living animals used deeply conserved innate immunity TFs to recognise and maintain a beneficial microbiome.

Introduction

The animal innate immune system protects against pathogenic agents, while also playing a critical role in regulating interactions between animal hosts and their microbial symbionts (Bosch 2012; Hentschel et al. 2012; Chu and Mazmanian 2013; McFall-Ngai et al. 2013a; Gilbert et al. 2015; Schretter et al. 2018; Berg et al. 2019; Bosch et al. 2019; Dierking and Pita 2020; Hadfield and Bosch 2020; Nyholm and McFall-Ngai 2021; Bosch et al. 2024). Indeed, the latter may be its ancestral role, given that animals originated in an aqueous environment already dense with

microbes, and thus required mechanisms to discriminate beneficial from non-beneficial bacteria (McFall-Ngai et al. 2013b; Alegado and King 2014; Woznica and King 2018; Richter and Levin 2019)

In general, the development and spatial management of microbial symbionts begins with pattern recognition receptors (PRRs) on or in those cells that have first contact with the microbes, which in turn activate transcription factor (TF)-mediated gene regulatory networks (Janeway and Medzhitov 2002; Akira et al. 2006; Bosch et al. 2009; Nyholm and Graf 2012; Chu and Mazmanian 2013; Bosch 2014; Broderick 2016; Chen et al. 2019; Colosimo et al. 2019; Heppert et al. 2021).

Basal invertebrate animals share many innate immunity genes and some immune responses with vertebrates, and most animal innate immune TFs are likely to have been present in the last common ancestor of all living animals (Hemmrich et al. 2007; Miller et al. 2007; Bosch et al. 2009; Srivastava et al. 2010; Hentschel et al. 2012b; Bosch 2014; Yuen et al. 2014). Despite this, it is unclear if regulatory mechanisms for responding to disparate microbes are as deeply conserved and ancient as the existence of animal-bacterial interactions. Specifically, it has not yet been determined if conserved immunity TFs ancestrally functioned to coordinate differential responses to symbionts compared to potential pathogens (Miller et al. 2007; Mansfield and Gilmore 2019; Williams and Gilmore 2020; Silva and Gomes 2024a). Understanding these regulatory mechanisms has become a pressing question in modern biology, with the recent realisation that animal-bacterial symbioses are ubiquitous across metazoans and often critical to healthy function of individuals through to the ecosystems they inhabit.

Filter-feeding marine invertebrates, such as sponges (phylum Porifera), are valuable systems for addressing this question of TF-mediated mechanisms, because they must acquire their nutrition from environmental microbes while simultaneously protecting against potential pathogens and maintaining a healthy symbiotic microbiome (Fan et al. 2012; Hentschel et al. 2012; Thomas et al. 2016). As a consequence, they have a constitutively active innate immune system that is poised to react rapidly and differentially to environmental and symbiotic microbes (Williams and Gilmore 2022). Furthermore, sponges represent one of the earliest phyletic lineages to diverge from the rest of the animal kingdom. Thus traits shared between sponges and bilaterians can logically be traced back to their last common ancestor and so reveal conserved features that could have been inherited by all extant animals.

In this context, here we investigate the molecular pathways used by a marine demosponge, *Amphimedon queenslandica*, to discriminate native symbiotic bacteria from foreign bacteria. Sponges are composed of an epithelial boundary covering an internal collagenous layer that houses a diversity of phagocytic, secretory and structural cells (Leys and Hill 2012a; Dunn et al. 2015; Sebé-Pedrós et al. 2018a; Musser et al. 2021a; Ereskovsky et al. 2025a; Leys et al. 2025). Although sponges are one of the oldest phyletic lineages, diverging from bilaterians and cnidarians (parahoxozoans) some 700 million years ago, the sponge genome includes an expanded and

diversified repertoire of innate immunity TF, PRR and signalling pathway genes (Hentschel et al. 2012; Grice et al. 2017; Erwin 2020).

Results

Sponges host distinct bacterial communities

Sponges have species-specific bacterial communities that differ from surrounding environmental microbes, and tend to be either high or low in complexity and abundance (Fan et al. 2012; Hentschel et al. 2012; Gloeckner et al. 2014; Thomas et al. 2016). *Amphimedon queenslandica* (Figure 1A, B) has a microbiome that is low in complexity and abundance, dominated through its life cycle by three vertically-inherited symbiotic gammaproteobacteria – hereafter referred to as *AqS1*, *AqS2* and *AqS3* – that together can comprise up to 95% of the microbiome (Fieth et al. 2016; Gauthier, Watson, and Degnan 2016b) (Figure 1C). Unhealthy individuals in the wild are identified by their lower cellular mass and weak coloration (Figure 1B), associated with a reduced relative abundance of the core symbionts that suggests the beginning of microbiome dysbiosis (Figure 1C and Table S1). The sponge *Rhabdastrella globostellata*, which is co-located with *A. queenslandica* on coral reefs but is evolutionary distant, hosts a very different and more complex bacterial community that does not include *AqS1*, *AqS2* or *AqS3* (Figure 1C, D and Table S1).

Native and foreign bacteria are processed differently, and induce markedly different transcriptional responses in *Amphimedon*

CFDA-SE-labelled bacteria enriched from healthy and unhealthy *A. queenslandica* (referred to hereafter as healthy and unhealthy native bacteria) and from *R. globostellata* (referred to as foreign bacteria) were introduced separately into 0.2 µm filtered seawater (FSW) surrounding juvenile *A. queenslandica* (Figure 1E). Within 30 min of exposure, native and foreign bacteria were observed in choanocytes – internal flagellated epithelial cells that draw water through the sponge body and capture bacteria (Maldonado 2004; Leys and Hill 2012b) – and in small amoeboid cells that have filopodial contacts with the basal surface of these choanocytes (Figure 1 and Figure S1). By 1.5 hours later (2 hours post-exposure; hpe) only native bacteria had been transferred to the phagocytic pluripotent amoeboid cells, called archaeocytes, that move through the internal mesohyl ($p < 0.01$) (Figure 2G-I). Strikingly more archaeocytes contain bacteria from healthy compared to unhealthy *A. queenslandica* ($p < 0.01$) (Figure 2G, H, J and Figure S2), consistent with this sponge having a finely tuned system to rapidly discern native from foreign bacteria and levels of dysbiosis. By 8 hpe, both native and foreign bacteria are detected in archaeocytes (Figure S2).

Given the strikingly different responses of *A. queenslandica* juveniles to healthy and unhealthy native bacteria, and to foreign bacteria, within just the first two hours of exposure, we compared transcriptomes of individual juveniles exposed for 2 and 8 hours to a bacterial enrichment with those maintained only in FSW (Table S2). Principle component analysis (PCA) of biologically-replicated transcriptomes reveals that the sponge has markedly different responses to native and foreign microbes, with about twice as many genes being significantly differentially

expressed in juveniles exposed to healthy native bacteria compared to foreign bacteria (DESeq2, *p*-adj < 0.05; Figure 2A-E, Figure S3 and Table S3). The transcriptional response to healthy native bacteria is transient and largely reverts to pre-exposure (FSW) levels already by 8 hpe. Although bacteria from unhealthy *A. queenslandica* induce similar changes in gene expression, the transcriptional response is markedly weaker and slower. This muted response correlates with slower transfer of unhealthy native bacteria to archaeocytes (Figure 1J) and is consistent with the host sponge recognising subtle differences in its microbiome composition that may indicate early signs of dysbiosis, and attenuating its response accordingly.

Native bacteria induce a rapid and transient innate immunity response

Native bacteria from healthy sponges significantly affect the expression of over 80 TFs by 2 hpe (*p*-adj < 0.05), with most reverting back to pre-exposure (FSW) transcript levels by 8 hpe (Figure 2C), demonstrating *A. queenslandica* juveniles are poised to rapidly recognise and transcriptionally respond to their native symbionts. The timing of this response correlates with the first transfer of native bacteria to archaeocytes (Figure 1). The differentially expressed TFs are enriched in the epithelial choanocytes and pinacocytes of adults, which have similar expression profiles to juveniles (Gaiti et al. 2017; Sogabe et al. 2019). Pinacocytes and choanocytes are the first sponge cells to contact external bacteria (Figure S5 and Table S5).

TFs with conserved roles in metazoan innate immunity that are upregulated in response to native symbionts at 2 hpe include NF-κB, two IRFs, STAT, two SMADs, AP1, three Fox genes and a nuclear receptor (NR). Strikingly, all members of ETS and 13 of 17 bZIP families are activated by native bacteria. *NF-κB*, *IRF*, *STAT*, *SMAD1/5*, *SMAD3*, *ATF2*, *Oasis A* and *Oasis B* transcript levels induced by bacteria from unhealthy *A. queenslandica* increase more slowly, such that the 8 hpe levels are similar to the 2 hpe response to bacteria from healthy individuals (Figure 2C), matching the more prolonged overall transcriptional response and the slower cellular processing of these bacteria.

PRR expression induced by native bacteria closely matches that of the TFs and includes the transient activation or repression of 56 scavenger receptor cysteine-rich domain-containing (SRCR), 32 G protein-coupled receptor (GPCR) and 50 immunoglobulin superfamily (IgSF) genes (Figure 2D, Figure S3 and Table S3). Amongst receptors induced by native symbionts are AmqIgTIR1 and 2, which are significantly up and down regulated, respectively, and are comprised of extracellular IL1R-like Igs and an intracellular TLR-like Toll/interleukin1 domain (Gauthier, Pasquier and Degnan 2010). Multiple sponge-specific GPCRs with close affinity to parahoxozoan γ-aminobutyric acid (GABA) receptors also are induced by native bacteria. GABA can be synthesised and degraded by *AqS1* and is involved in host-microbe interactions in other animal holobionts (Figure S3) (Krishnan et al. 2015; Xiang 2021; Shekarabi et al. 2024). By contrast, multiple CL163-L1 SRCRs are upregulated in *A. queenslandica* exposed to foreign bacteria; this type of SRCR is upregulated in mammalian macrophages during inflammation (Gorp et al. 2010). Both the GABA- and CL163-like receptors are most highly expressed in epithelial pinacocytes and choanocytes in adults, consistent with these cells constitutively expressing PRRs to detect both native and foreign bacteria (Figure S5).

Genes encoding conserved members of innate immunity pathways are also transiently activated at 2 hpe by native symbionts from healthy *A. queenslandica* (Figure 2D, Figure S3 and Table S3). This includes the differential expression of eight TRAFs of the pro-inflammatory cytokine TNF pathway, and Toll, Imd, apoptosis, TGF-β and JAK-STAT pathways. These immunity pathway genes are also largely expressed constitutively in adult epithelial pinacocytes and choanocytes (Figure S5 and S6 and Tables S5).

There are markedly fewer innate immunity genes induced by foreign bacteria, and these are largely expressed at lower levels and less transiently (Figure 2, Figure S3 and Table S3). For instance, amongst the PRR genes that are differentially expressed at 2 hpe (p-adj < 0.05), 94.5% and 30.8% are induced by native and foreign bacteria, respectively. In addition to this weaker innate immune response, the prolonged response to foreign bacteria includes the activation of genes involved in xenobiotic metabolism (Figure 2E). By contrast to innate immunity genes, xenobiotic genes activated by the foreign microbes are chiefly constitutively expressed in internal archaeocytes (Figure S5 and Table S5).

IRF, NF-κB and STAT appear central to sponge-symbiont interactions

A multivariate sparse partial least squares discriminant analysis (sPLS-DA) and a weighted gene co-expression network analysis (WGCNA) of genes expressed in bacterial treatment together identified genes most likely to contribute to *A. queenslandica*'s rapid innate immune response to its native bacteria. 99% of the genes identified by sPLS-DA overlap with those identified using DESeq2 (Figure 2B, Figure S4 and Table S4). Two of the six WGCNA co-expression modules are comprised of genes that are induced at 2 hpe by native symbiotic bacteria, with module 1 having nearly all the activated innate immunity genes identified by DESeq2 and sPLS-DA (Figure 2F, Figure S7 and Table S6). Most of the other highly connected genes in this co-expression network have conserved roles in innate immunity (e.g. TRAF, Myd88 and IgTIR1). Genes involved in endocytosis and vesicle trafficking are co-expressed with the immunity genes induced by native bacteria.

IRF, NF-κB and STAT appear to be the most connected TFs in the native bacterial-induced co-expression network, and thus likely to play a central in the response to native symbionts (Figure 2F). We thus generated antibodies against these three TFs to determine their roles in gene regulation at the time when we see native bacteria differentially present in archaeocytes, and a marked change in innate immunity gene expression (i.e., 2 hpe; Figs 1 and 2).

IRF, NF-κB and STAT are present in the cytoplasm of choanocytes of juveniles maintained only in FSW, with IRF being more apically localized in the microvillar collar of these cells compared to the other two TFs (Figure 3A-D and Figure S8). IRF, NF-κB and STAT are also present in the cytoplasm of amoebocytes adjacent to choanocyte chambers, and NF-κB is constitutively nuclear localized in a subset of archaeocytes in the vicinity of choanocyte chambers (Figure 3B, D). At 2 hpe, these TFs remain localized to choanocyte cytoplasm regardless of whether exposed to native or foreign bacteria (Figure 3E-L). By contrast, IRF translocates to the nuclei of small amoebocytes that have engulfed native bacteria, but remains cytoplasmic when these cells engulf foreign bacteria,

appearing to co-localize with the foreign bacteria (Figure 3E, I). This suggests that IRF in these proximal amoebocytes is playing a central role in the initial discrimination of native from foreign bacteria. We did not detect NF-κB or STAT in the nuclei of these amoebocytes in either native or foreign bacterial treatments. However, NF-κB co-localises with IRF in nuclei of amoebocytes that have engulfed native bacteria but are no longer in direct contact with choanocyte chambers (Figure 3F-H, J-L), suggesting NF-κB nuclear localization follows IRF in the same amoeboid cells that initially engulfed symbiotic bacteria. Interestingly, STAT is induced by native bacteria to translocate into the nuclei of a different subset of amoebocytes that are not associated with choanocyte chambers and do not appear to have engulfed bacteria (Figure 3G, H, K, L), suggesting this is induced by signalling event - JAK-STAT, Toll, Imd, FoxO, Wnt and TGF-β pathway components are upregulated at 2 hpe.

Discussion

The responses of the sponge *Amphimedon queenslandica* to symbiotic and foreign bacteria are markedly different in speed and scale, and provide strong support for the innate immune system being critical in sponge-symbiont interactions. The sponge appears poised to rapidly detect and transcriptionally respond to its symbionts, swiftly activating a suite of conserved innate immunity genes. This includes a wide array of TF families that have roles in innate immunity across the animal kingdom, such as IRF, STAT, NF-κB, AP-1 and other bZIPs, ETS, SMADs, and NRs (Honda and Taniguchi 2006; Glass and Natoli 2016; Platanitis and Decker 2018; Bejjani et al. 2019; Williams et al. 2019; Kusiak and Brady 2022; Silva and Gomes 2024b). Notably, this conservation of TFs in immunity appears to be more striking than in TFs that regulate animal development. That is, both sponge and ctenophore basal lineages have many orthologues of TFs that are highly conserved in bilaterian developmental (Degnan et al. 2015; Levin et al. 2016; Cornejo-Páramo et al. 2022), but their expression in these basal phyla appears to differ from those conserved roles (Reitzel, Pang, and Martindale 2016; Srivastava et al. 2010). This suggests that the transcriptional regulation of holobiont fidelity by the innate immune system predates the ontogenetic life cycle of animals, with ancestral immunity genes being co-opted into developmental roles later in metazoan evolution, such as NF-κB and Toll pathway (Williams and Gilmore 2020, 2022; Gauthier, Pasquier, and Degnan 2010; Gauthier and Degnan 2008). IRF, AP-1, ETS, SMAD and NR families appear to have evolved in after the divergence of animal and choanoflagellate lineages. Thus, the regulation of symbionts appears paramount and unique to the metazoan multicellular condition (Wilde et al. 2024)

Sponges have no gut, nor nerve and muscle cells, but do have an epithelium and internal phagocytic amoeboid cells that are akin, and arguably homologous, to cell types present in other animals (Srivastava et al. 2010; Musser et al. 2021; Ereskovsky, Melnikov, and Lavrov 2025; Leys and Hill 2012b). The constitutive expression of many conserved immunity TF, PRR and signalling genes in the epithelium – sponge pinacocytes and choanocytes – indicates that these cells are poised to discriminate native from foreign bacteria. Given this and the tight alliance of symbionts

and epithelia in disparate animals (Bosch 2012; McFall-Ngai et al. 2013a; Bosch et al. 2019; Maritan et al. 2024), it appears that the epithelial cell layer has been instrumental in rapidly discriminating beneficial, harmful and neutral bacteria, and probably has been shaping host-symbiont interactions since before the origin of the gut.

IRF appears to be central to the differential response of the sponge to native and foreign bacteria, beginning in small phagocytic amoebocytes that receive native and foreign bacteria from epithelial choanocytes. IRF translocates to the nucleus only in response to native symbionts, consist with these cells being primed to discriminate native from foreign bacteria and activate a transcriptional response. IRF remains in the cytoplasm in sponge amoebocytes that have engulfed foreign bacteria, appearing to co-localise with these bacteria. This is consistent with observations in macrophages and other cell types, where IRF binds to MyD88 on the surface of endosomes and has a non-TF signalling role (Honda et al. 2005; Honda and Taniguchi 2006; Ikushima et al. 2014; Fitzgerald and Kagan 2020).

NF-κB translocates into the nuclei of symbiont-carrying amoebocytes shortly after IRF, suggesting it also contributes to regulation of symbiont processing. Indeed, IRFs and NF-κB regulate the swift transcriptional responses in other animal cells upon stimulation of Toll-like receptors and other PRRs (Honda and Taniguchi 2006; Ahmad et al. 2024). Our findings that these two TFs, along with STAT, appear central to the transcriptional response of *A. queenslandica* to its symbionts, strongly suggest an ancestral role for IRF, NF-κB and STAT in the immediate discrimination of beneficial symbionts from foreign bacteria evolved very early in metazoans. Based on single cell transcriptomics, these small phagocytic amoebocytes appear to have macrophage-like properties and play a role in sponge defence (Sebé-Pedrós et al. 2018b; Musser et al. 2021b) suggesting this cell type was present in the LCA of sponges and parahoxozoans.

In conclusion, we have empirically demonstrated that sponges, like more complex animals, use innate immunity TFs to regulate their microbiome. This occurs rapidly and adjacent to the sponge epithelial layer, consistent with the immune system of aquatic filter-feeding animals being poised to differentially respond to beneficial, harmful and neutral bacteria. Given the basal phylogenetic position of sponges, this suggests that the earliest animals first used the innate immune system to recognize symbionts from foreign bacteria and thus to maintain holobiont fidelity. The muted, yet longer-lasting, activation of these genes by symbionts derived from unhealthy and dying sponges is consistent with the LCA of animals possessing a finely tuned innate immune system that could respond to subtle dysbiotic situations to maintain a beneficial microbiome.

Materials and methods

Enrichment and characterisation of sponge bacterial communities

Amphimedon queenslandica and *Rhabdastrella globostellata* were collected from Heron Island Reef, Great Barrier Reef, Australia (23°27′S, 151°55′E) (Figure 1A, B, D), and

bacterial communities were enriched from individual sponges as previously described (Gauthier, Watson, and Degnan 2016a; Thomas et al. 2010). The health of *A. queenslandica* individuals was visually assessed in the field prior to collection. Healthy individuals were grey and had high cellular mass, while unhealthy individuals had body regions that were pale brown to olive colour and had a lower cell mass and regions of exposed extracellular matrix (Figure 1A, B). *A. queenslandica* and *R. globostellata* bacterial enrichments were diluted in 0.2 µm filtered sea water (FSW) to approximate final concentration of 10^7 cells/ml. DNA was extracted from approximately 10^6 cells of these bacterial enrichments to identify prokaryotic operational taxonomic units (OTUs) via 16S rRNA gene amplicon sequencing as previously described (Fieth et al. 2016).

Rearing *A. queenslandica* larvae and juveniles

Naturally-released *A. queenslandica* larvae were collected in larval traps from 25 individuals, pooled and maintained in ambient seawater for 6-8 h before being induced to settle on the coralline alga *Amphiroa fragilissima* (Ueda et al. 2016; Say and Degnan 2020) Within 6 h of settling on *A. fragilissima*, *A. queenslandica* postlarvae were detached from the algae and resettled individually onto glass coverslips (Sogabe et al. 2019) . These were placed in sterile 24-well plates in 2 ml FSW and reared for 96 h at 25°C until reaching the juvenile stage with a functional aquiferous system (Degnan et al. 2015).

Labelling and tracing bacteria in juvenile sponges

Bacterial enrichments were centrifuged at 5000 x g for 10 min and resuspended in 1 ml of 5 µM carboxyfluorescein diacetate succinimidyl ester (CFDA-SE; Vybrant, Thermofisher Scientific) in FSW. After incubating for 15 min at room temperature, the cell suspensions were centrifuged at 5000 x g for 10 min. The pellets were washed twice in FSW, resuspended in 1 ml FSW and maintained at 4°C in the dark. Juvenile *A. queenslandica* were washed in FSW and the volume of FSW in each well was adjusted to 1.5 ml. 40 µL of the CFDA-SE labelled microbial enrichments from either a healthy or unhealthy *A. queenslandica*, or *R. globostellata* were introduced to the FSW in each well, yielding final concentrations of 2.8, 3.6 or 2.7×10^4 cells/ml, respectively. Control treatments were juveniles receiving 40 µl FSW. Juveniles were then cultivated in the presence of the labelled bacteria in the dark. Individual juveniles were fixed 0.5, 1, 2 and 8 h post-exposure (hpe) as previously described (Larroux et al. 2008) . For the 8 hpe incubations, the wells were washed once with fresh FSW after 2 h and the juveniles were reared in FSW for the last 6 h. Fixed juveniles were labelled with 4,6-diamidino-2-phenylindole (DAPI; 1:1000, Molecular Probes), mounted in ProLong Gold anti-fade reagent (Molecular Probes) and observed and photographed using a Zeiss LSM 510 META confocal microscope (Sogabe et al. 2016) .

The number of choanocyte chambers, archaeocytes and microbe-containing archaeocytes were counted in four randomly-chosen confocal sections obtained from the inner cortex of five juveniles (n = 20) exposed to the bacterial enrichment for 0.5, 1, 2 and 8 h. A one-way ANOVA followed by the Tukey's HSD post-hoc tests were performed on the data obtained from juveniles fed with enrichments from health and unhealthy *A. queenslandica*, and *R. globostellata*.

CEL-seq2 analysis of juvenile transcriptomes

Individual juvenile *A. queenslandica* were exposed to bacterial enrichments from healthy or unhealthy *A. queenslandica* (native), *R. globostellata* (foreign), or FSW for 2 or 8 h as described above. At 0, 2 and 8 hpe, juveniles were individually transferred to 300 µl of RNALater (Sigma), stored overnight at 4°C and then at -20°C. RNA was extracted from each juvenile using the EZ Spin Column Total RNA Isolation Kit (BioBasic Inc., Toronto, Canada) according to the manufacturer's instructions, and amplified and sequenced using the CEL-seq2 method (Hashimshony et al. 2016) . The CEL-seq2 samples were multiplexed, resulting in the generation of two libraries, which were sequenced over two sequencing runs on an Illumina HiSeq2500, with samples from each treatment group and time point divided between the two runs (Table S2). CEL-seq2 reads were processed using a publicly available pipeline (https://github.com/yanailab/CEL-Seq-pipeline) and the demultiplexed raw reads were mapped to the *A. queenslandica* genome and gene-level read counts were generated using Aqu 2.1 gene models (Fernandez-Valverde et al. 2015) (Table S2). All data are available at NCBI Bioproject PRJNA1121035 (*available from June 1 2025*).

Analysis of gene expression

Differential gene expression analysis was performed with the CEL-seq2 mapped read counts using the Bioconductor package DESeq2 (Love et al. 2014) . Genes with median read counts less than 10 were filtered out before analysis. Blind variance stabilizing transformation (VST) and principal component analysis (PCA) was conducted on the read counts (Love et al. 2014) . The results of the unsupervised PCA analysis were visualised by a scatter plot derived from ggplot2 (Wickham 2016). Differentially expressed genes, with adjusted *p*-value < 0.05, were identified by pairwise comparisons between each treatment group and the corresponding FSW control. An UpSet plot generated by R packages ComplexUpset and ggplot2 was utilized to visualise the number of differentially expressed genes within each treatment group and the intersection across groups (Lex et al. 2014; Wickham 2016). Heatmaps generated by ComplexHeatmap based on inter-group normalised VST counts were used to visualise the relative expression changes of differentially expressed genes (Gu et al. 2016).

Sparse partial least squares discriminant analysis (sPLS-DA), a supervised machine learning method integrated into the mixOmics package (Rohart et al. 2017) , was used to identify

expressed genes featured in juveniles exposed to bacterial enrichments. The predictive model was first trained using the 2 hpe datasets by repeating the 3-fold cross-validation method 50 times. Then, the trained model was used to predict the bacterial type of the 8 hpe bacterial datasets, and only datasets with the correct bacterial type were retained. Finally, sPLS-DA was performed on the combined datasets consisting of the retained 8 hpe datasets and the full 2 hpe datasets to identify feature genes for native and foreign bacteria on each principal component level. The scatter plot of samples with 95% confidence ellipses generated by the R package ggplot2 based on the sPLS-DA model was used to visualise the differences among treatment groups and the similarities within groups. The Bioconductor package ComplexHeatmap was used to generate heatmaps based on VST counts, to visualise the relative expression variations of the two PCs feature genes, respectively.

A weighted co-expression analysis of gene expression profiles was undertaken using the R package WGCNA (Langfelder and Horvath 2008), on VST counts obtained from DESeq2 that first were filtered by mean expression and variance; VST counts of a total of 8457 genes with median or median absolute deviation ranking in the top 5000 were retained. With β of 3 as soft thresholding, genes with distinct expression profiles were grouped into various modules, and a weighted co-expression network of the genes within the module was identified. Specifically, these networks were constructed based on the signed Nowick-type of topological overlap metric, which was used to cluster the modules using the dynamic tree cut algorithm with a height of 0.15 and a minimum module size of 100. Co-expressed gene modules were identified by the hierarchical clustering method. The relative gene expression profile of each co-expressed gene module was visualised by the R package ggplot2. Module eigengenes (MEs) were correlated to bacterial treatments and time points, and modules with p-values < 0.05 were identified as those significantly correlated with the corresponding groups. ME and group relationships were visualised using ggplot2 and ComplexHeatmap, respectively (Gu et al. 2016; Wickham 2016).

GO and KEGG Pathway enrichment analyses

The gene ontology (GO) and Kyoto Encyclopedia of Genes and Genomes (KEGG) biological pathway terms of all protein coding genes were obtained by annotating the predicted proteome of *A. queenslandica* with the online genome functional annotation tool eggNOG-mapper (http://eggnog-mapper.embl.de) (Cantalapiedra et al. 2021). Enrichment analysis of KEGG pathway terms was performed for each module using a one-sided version of Fisher's exact test built in the Bioconductor package clusterProfiler (Wu et al. 2021) . The p-value was adjusted by the FDR method to obtain the corresponding q-value, which was less than 0.05 for significantly enriched KEGG pathways. Based on the results of KEGG pathway enrichment analysis, the distribution of significantly enriched terms across modules was visualised with heatmaps generated by ggplot2 (Wickham 2016).

Immunofluorescence

Juveniles were fixed at 2 hpe for immunofluorescence analyses using antisera raised against IRF, NF-kB and STAT peptide epitopes (Yang et al. 2024). Rabbit polyclonal antisera against *A. queenslandica* IRF (TRSGSSADEQEPERPER), STAT (QRLFNHEDDPNRNE) and NF-κB (NGIDPSSLPEALIR) peptide epitopes were produced by GenScript (Piscataway, New Jersey, U.S). These antisera were individually diluted 1:500 in the fresh blocking buffer and incubated with the fixed juveniles overnight at 4°C as previously described (Yang et al. 2024).

References

Ahmad Z, Kahloan W, Rosen ED. 2024. Transcriptional control of metabolism by interferon regulatory factors. *Nat. Rev. Endocrinol.* 20:573–587.

Akira S, Uematsu S, Takeuchi O. 2006. Pathogen recognition and innate immunity. *Cell* 124:783–801.

Alegado RA, King N. 2014. Bacterial influences on animal origins. *Cold Spring Harb. Perspect. Biol.* 6:a016162–a016162.

Bejjani F, Evanno E, Zibara K, Piechaczyk M, Jariel-Encontre I. 2019. The AP-1 transcriptional complex: Local switch or remote command? *Biochim. Biophys. Acta (BBA) - Rev. Cancer* 1872:11–23.

Berg M, Monnin D, Cho J, Nelson L, Crits-Christoph A, Shapira M. 2019. TGFβ/BMP immune signaling affects abundance and function of *C. elegans* gut commensals. *Nat. Commun.* 10:604.

Bosch TCG. 2012. Cnidarian-microbe interactions and the origin of innate immunity in metazoans. *Annu. Rev. Microbiol.* 67:499–518.

Bosch TCG. 2014. Rethinking the role of immunity: lessons from Hydra. *Trends Immunol.* 35:495–502.

Bosch TCG, Augustin R, Anton-Erxleben F, Fraune S, Hemmrich G, Zill H, Rosenstiel P, Jacobs G, Schreiber S, Leippe M, et al. 2009. Uncovering the evolutionary history of innate immunity: The simple metazoan Hydra uses epithelial cells for host defence. *Dev. Comp. Immunol.* 33:559–569.

Bosch TCG, Blaser MJ, Ruby E, McFall-Ngai M. 2024. A new lexicon in the age of microbiome research. *Philos. Trans. R. Soc. B* 379:20230060.

Bosch TCG, Guillemin K, McFall-Ngai M. 2019. Evolutionary “experiments” in symbiosis: The study of model animals provides insights into the mechanisms underlying the diversity of host–microbe interactions. *Bioessays* 41:1800256.

Broderick NA. 2016. Friend, foe or food? Recognition and the role of antimicrobial peptides in gut immunity and *Drosophila*–microbe interactions. *Philos. Tran. R. Soc. B* 371:20150295–10.

Cantalapiedra CP, Hernández-Plaza A, Letunic I, Bork P, Huerta-Cepas J. 2021. eggNOG-mapper v2: Functional annotation, orthology assignments, and domain prediction at the metagenomic scale. *Mol. Biol. Evol.* 38:5825–5829.

Chen H, Nwe P-K, Yang Y, Rosen CE, Bielecka AA, Kuchroo M, Cline GW, Kruse AC, Ring AM, Crawford JM, et al. 2019. A forward chemical genetic screen reveals gut microbiota metabolites that modulate host physiology. *Cell* 177:1217-1231.e18.

Chu H, Mazmanian SK. 2013. Innate immune recognition of the microbiota promotes host-microbial symbiosis. *Nat. Immunol.* 14:668–675.

Colosimo DA, Kohn JA, Luo PM, Piscotta FJ, Han SM, Pickard AJ, Rao A, Cross JR, Cohen LJ, Brady SF. 2019. Mapping interactions of microbial metabolites with human G-protein-coupled receptors. *Cell Host Microbe* 26:273-282.e7.

Cornejo-Páramo P, Roper K, Degnan SM, Degnan BM, Wong ES. 2022. Distal regulation, silencers, and a shared combinatorial syntax are hallmarks of animal embryogenesis. *Genome Res.* 32:474–487.

Degnan BM, Adamska M, Richards GS, Larroux C, Leininger S, Bergum B, Calcino A, Taylor K, Nakanishi N, Degnan SM. 2015. Porifera. In: *Evolutionary Developmental Biology of Invertebrates 1*. Springer Vienna. p. 65–106.

Dierking K, Pita L. 2020. Receptors mediating host-microbiota communication in the metaorganism: The invertebrate perspective. *Front. Immunol.* 11:185–17.

Dunn CW, Leys SP, Haddock SHD. 2015. The hidden biology of sponges and ctenophores. *Trends Ecol. Evol.* 30:282–291.

Ereskovsky A, Melnikov NP, Lavrov A. 2025. Archaeocytes in sponges: simple cells of complicated fate. *Biol. Rev.* 100:790–814.

Erwin DH. 2020. The origin of animal body plans: a view from fossil evidence and the regulatory genome. *Development* 147:dev182899-14.

Fan L, Reynolds D, Liu M, Stark M, Kjelleberg S, Webster NS, Thomas T. 2012. Functional equivalence and evolutionary convergence in complex communities of microbial sponge symbionts. *Proc. Nal Acad. Sci. USA* 109:E1878–E1887.

Fernandez-Valverde SL, Calcino AD, Degnan BM. 2015. Deep developmental transcriptome sequencing uncovers numerous new genes and enhances gene annotation in the sponge *Amphimedon queenslandica*. *BMC Genomics* 16:720–11.

Fieth RA, Gauthier M-EA, Bayes J, Green KM, Degnan SM. 2016. Ontogenetic changes in the bacterial symbiont community of the tropical demosponge *Amphimedon queenslandica*: Metamorphosis is a new beginning. *Front. Mar. Sci.* 3:3022–20.

Fitzgerald KA, Kagan JC. 2020. Toll-like receptors and the control of immunity. *Cell* 180:1044–1066.

Gaiti F, Jindrich K, Fernandez-Valverde SL, Roper KE, Degnan BM, Tanurdzic M. 2017. Landscape of histone modifications in a sponge reveals the origin of animal cis-regulatory complexity. *eLife* 6:e366.

Gauthier M, Degnan BM. 2008. The transcription factor NF-κB in the demosponge *Amphimedon queenslandica*: insights on the evolutionary origin of the Rel homology domain. *Dev. Genes Evol.* 218:23–32.

Gauthier MEA, Pasquier LD, Degnan BM. 2010. The genome of the sponge *Amphimedon queenslandica* provides new perspectives into the origin of Toll-like and interleukin 1 receptor pathways. *Evol. Dev.* 12:519 –533

Gauthier MEA, Watson JR, Degnan SM. 2016. Draft genomes shed light on the dual bacterial symbiosis that dominates the microbiome of the coral reef sponge *Amphimedon queenslandica*. *Front. Mar. Sci.* 3:196.

Gilbert SF, Bosch TCG, Ledon-Rettig C. 2015. Eco-Evo-Devo: developmental symbiosis and developmental plasticity as evolutionary agents. *Nat. Rev. Genet.* 16:611–622.

Glass CK, Natoli G. 2016. Molecular control of activation and priming in macrophages. *Nat. Immunol.* 17:26–33.

Gloeckner V, Wehrl M, Moitinho-Silva L, Gernert C, Schupp P, Pawlik JR, Lindquist NL, Erpenbeck D, Wörheide G, Hentschel U. 2014. The HMA-LMA dichotomy revisited: an electron microscopical survey of 56 sponge species. *Biol. Bull.* 227:78–88.

Gorp HV, Delputte PL, Nauwynck HJ. 2010. Scavenger receptor CD163, a Jack-of-all-trades and potential target for cell-directed therapy. *Mol. Immunol.* 47:1650–1660.

Grice LF, Gauthier MEA, Roper KE, Fernàndez-Busquets X, Degnan SM, Degnan BM. 2017. Origin and evolution of the sponge aggregation factor gene family. *Mol. Biol. Evol.* 34:msx058-1099.

Gu Z, Eils R, Schlesner M. 2016. Complex heatmaps reveal patterns and correlations in multidimensional genomic data. *Bioinformatics* 32:2847–2849.

Hadfield MG, Bosch TCG. 2020. Cellular dialogues between hosts and microbial symbionts. In: *Cellular Dialogues in the Holobiont*. CRC Press p. 287–290.

Hashimshony T, Senderovich N, Avital G, Klochendler A, Leeuw Y de, Anavy L, Gennert D, Li S, Livak KJ, Rozenblatt-Rosen O, et al. 2016. CEL-Seq2: sensitive highly-multiplexed single-cell RNA-Seq. *Genome Biol.* 17:77.

Hentschel U, Piel J, Degnan SM, Taylor MW. 2012. Genomic insights into the marine sponge microbiome. *Nat. Rev. Microbiol.* 10:641–654.

Heppert JK, Davison JM, Kelly C, Mercado GP, Lickwar CR, Rawls JF. 2021. Transcriptional programmes underlying cellular identity and microbial responsiveness in the intestinal epithelium. *Nat. Rev. Gastroentero.* 18:7–23.

Honda K, Ohba Y, Yanai H, Negishi H, Mizutani T, Takaoka A, Taya C, Taniguchi T. 2005. Spatiotemporal regulation of MyD88–IRF-7 signalling for robust type-I interferon induction. *Nature* 434:1035–1040.

Honda K, Taniguchi T. 2006. IRFs: master regulators of signalling by Toll-like receptors and cytosolic pattern-recognition receptors. *Nat. Rev. Immunol.* 6:644–658.

Ikushima H, Negishi H, Taniguchi T. 2014. The IRF family transcription factors at the interface of innate and adaptive immune responses. *Cold Spring Harb. Symp. Quant. Biol.* 78:105–116.

Janeway CA, Medzhitov R. 2002. Innate immune recognition. *Immunology* 20:197–216.

Krishnan A, Dnyansagar R, Almén MS, Williams MJ, Fredriksson R, Manoj N, Schiöth HB. 2015. The GPCR repertoire in the demosponge *Amphimedon queenslandica*: insights into the GPCR system at the early divergence of animals. *BMC Evol. Biol.* 14:270.

Kusiak A, Brady G. 2022. Bifurcation of signalling in human innate immune pathways to NF-kB and IRF family activation. *Biochem. Pharmacol.* 205:115246.

Langfelder P, Horvath S. 2008. WGCNA: an R package for weighted correlation network analysis. *BMC Bioinform.* 9:559–559.

Larroux C, Fahey B, Adamska M, Richards GS, Gauthier M, Green K, Lovas E, Degnan BM. 2008. Whole-mount in situ hybridization in *Amphimedon*. *Cold Spring Harb. Protoc.* 2008:pdb.prot5096.

Levin M, Anavy L, Cole AG, Winter E, Mostov N, Khair S, Senderovich N, Kovalev E, Silver DH, Feder M, et al. 2016. The mid-developmental transition and the evolution of animal body plans. *Nature* 531:637–641.

Lex A, Gehlenborg N, Strobelt H, Vuillemot R, Pfister H. 2014. UpSet: Visualization of Intersecting Sets. *IEEE Trans. Vis. Comput. Graph.* 20:1983–1992.

Leys SP, Grombacher L, Field D, Elliott GRD, Ho VR, Kahn AS, Reid PJ, Riesgo A, Lanna E, Bobkov Y, et al. 2025. A morphological cell atlas of the freshwater sponge *Ephydatia muelleri* with key insights from targeted single-cell transcriptomes. *EvoDevo* 16:1.

Leys SP, Hill A. 2012. The physiology and molecular biology of sponge tissues. *Adv. Mar. Biol.* 62:1–56.

Love MI, Huber W, Anders S. 2014. Moderated estimation of fold change and dispersion for RNA-seq data with DESeq2. *Genome Biol.* 15:550.

Maldonado M. 2004. Choanoflagellates, choanocytes, and animal multicellularity. *Invertebrate Biology* 123:1–22.

Mansfield KM, Gilmore TD. 2019. Innate immunity and cnidarian-Symbiodiniaceae mutualism. *Dev. Comp. Immunol.* 90:199–209.

Maritan E, Quagliariello A, Frago E, Patarnello T, Martino ME. 2024. The role of animal hosts in shaping gut microbiome variation. *Philos. Trans. R. Soc. B* 379:20230071.

McFall-Ngai M, Hadfield MG, Bosch TCG, Carey HV, Domazet-Lošo T, Douglas AE, Dubilier N, Eberl G, Fukami T, Gilbert SF, et al. 2013a. Animals in a bacterial world, a new imperative for the life sciences. *Proc. Natl Acad. Sci.* 110:3229–3236.

Musser JM, Schippers KJ, Nickel M, Mizzon G, Kohn AB, Pape C, Ronchi P, Papadopoulos N, Tarashansky AJ, Hammel JU, et al. 2021a. Profiling cellular diversity in sponges informs animal cell type and nervous system evolution. *Science* 374:717–723.

Nyholm SV, Graf J. 2012. Knowing your friends: invertebrate innate immunity fosters beneficial bacterial symbioses. *Nat. Rev. Microbiol.* 10:815–827.

Nyholm SV, McFall-Ngai MJ. 2021. A lasting symbiosis: how the Hawaiian bobtail squid finds and keeps its bioluminescent bacterial partner. *Nat. Rev. Microbiol.* 19:666–679.

Platanitis E, Decker T. 2018. Regulatory networks involving STATs, IRFs, and NFκB in inflammation. *Front. Immunol.* 9:2542.

Reitzel AM, Pang K, Martindale MQ. 2016. Developmental expression of “germline”- and “sex determination”-related genes in the ctenophore *Mnemiopsis leidyi*. *EvoDevo* 7:1–16.

Richter DJ, Levin TC. 2019. The origin and evolution of cell-intrinsic antibacterial defenses in eukaryotes. *Curr. Opin. Genet. Dev.* 58:111–122.

Rohart F, Gautier B, Singh A, Cao K-AL. 2017. mixOmics: An R package for ‘omics feature selection and multiple data integration. *PLoS Comput. Biol.* 13:e1005752.

Say TE, Degnan SM. 2020. Molecular and behavioural evidence that interdependent photo - and chemosensory systems regulate larval settlement in a marine sponge. *Mol. Ecol.* 29:247–261.

Schretter CE, Vielmetter J, Bartos I, Marka Z, Marka S, Argade S, Mazmanian SK. 2018. A gut microbial factor modulates locomotor behaviour in *Drosophila*. *Nature* 563:402–406.

Sebé-Pedrós A, Chomsky E, Pang K, Lara-Astiaso D, Gaiti F, Mukamel Z, Amit I, Hejnol A, Degnan BM, Tanay A. 2018a. Early metazoan cell type diversity and the evolution of multicellular gene regulation. *Nat. Ecol. Evol.* 2:1–17.

Shekarabi A, Qureishy I, Puglisi CH, Dalseth M, Vuong HE. 2024. Host–microbe interactions: communication in the microbiota–gut–brain axis. *Curr. Opin. Microbiol.* 80:102494.

Silva RCMC, Gomes FM. 2024a. Evolution of the major components of innate immunity in animals. *J. Mol. Evol.* 92:3–20.

Sogabe S, Hatleberg WL, Kocot KM, Say TE, Stoupin D, Roper KE, Fernandez-Valverde SL, Degnan SM, Degnan BM. 2019. Pluripotency and the origin of animal multicellularity. *Nature* 570:1–20.

Sogabe S, Nakanishi N, Degnan BM. 2016. The ontogeny of choanocyte chambers during metamorphosis in the demosponge *Amphimedon queenslandica*. *EvoDevo* 7:6.

Srivastava M, Larroux C, Lu DR, Mohanty K., Chapman J, Degnan B, Rokhsar DS. 2010. Early evolution of the LIM homeobox gene family. *BMC Biol.* 8:e4

Srivastava M, Simakov O, Chapman J, Fahey B, Gauthier MEA, Mitros T, Richards GS, Conaco C, Dacre M, Hellsten U, et al. 2010. The *Amphimedon queenslandica* genome and the evolution of animal complexity. *Nature* 466:720–726.

Thomas T, Moitinho-Silva L, Lurgi M, Björk JR, Easson C, Astudillo-García C, Olson JB, Erwin PM, López-Legentil S, Luter H, et al. 2016. Diversity, structure and convergent evolution of the global sponge microbiome. *Nat. Commun.* 7:11870.

Thomas T, Rusch D, DeMaere MZ, Yung PY, Lewis M, Halpern A, Heidelberg KB, Egan S, Steinberg PD, Kjelleberg S. 2010. Functional genomic signatures of sponge bacteria reveal unique and shared features of symbiosis. *ISME J.* 4:1557–1567.

Ueda N, Richards GS, Degnan BM, Kranz A, Adamska M, Croll RP, Degnan SM. 2016. An ancient role for nitric oxide in regulating the animal pelagobenthic life cycle: evidence from a marine sponge. *Sci. Rep.* 6:37546.

Wickham H. 2016. ggplot2, Elegant Graphics for Data Analysis. *R*.

Wilde J, Slack E, Foster KR. 2024. Host control of the microbiome: Mechanisms, evolution, and disease. *Science* 385:eadi3338.

Williams LM, Gilmore TD. 2020. Looking Down on NF-κB. *Mol. Cell. Biol.* 40:e00104-20.

Williams LM, Gilmore TD. 2022. An innate ability: How do basal invertebrates manage their chronic exposure to microbes? *Plos Path.* 18:e1010897.

Williams LM, Inge MM, Mansfield KM, Rasmussen A, Afghani J, Agrba M, Albert C, Andersson C, Babaei Milad, Babaei Mohammad, et al. 2019. Transcription factor NF-κB in a basal metazoan, the sponge, has conserved and unique sequences, activities, and regulation. *Dev Comp Immunol* 104:103559.

Woznica A, King N. 2018. Lessons from simple marine models on the bacterial regulation of eukaryotic development. *Curr Opin Microbiol* 43:108–116.

Wu T, Hu E, Xu S, Chen M, Guo P, Dai Z, Feng T, Zhou L, Tang W, Zhan L, et al. 2021. clusterProfiler 4.0: A universal enrichment tool for interpreting omics data. *Innov.* 2:100141.

Xiang X. 2021. Investigating host-symbiont crosstalk in the coral reef demosponge *Amphimedon queenslandica*. PhD thesis, University of Queensland

Yang B, Degnan BM, Degnan SM. 2024. An improved whole-mount immunofluorescence protocol for juvenile *Amphimedon queenslandica*. Protocols io:dx.doi.org/10.17504/protocols.io.e6nvw1o2wlmk/v1

Figure legends

Figure 1. Source and cellular fate of native and foreign microbes in experimental juvenile *A. queenslandica*. (**A-D**) Microbes inhabiting *Amphimedon queenslandica* and *Rhabdastrella globostellata.* (**A**) Healthy and (**B**) unhealthy *A. queenslandica in situ*. (**C**) The relative abundance of symbionts *AqS1*, *AqS2* and *AqS3* and other bacterial operational taxonomic units (OTUs) in healthy and unhealthy *A. queenslandica*, and *R. globostellata* (see Table S1 for taxonomic lists). (**D**) *R. globostellata in situ.* (**E**) DIC and fluorescence micrograph of a DAPI-stained (blue) juvenile fed native bacteria labelled with CFDA-SE (green) at 8 hpe. (**F**) Confocal micrograph of the area surrounding a single choanocyte chamber (Ch) from the same juvenile. Microbes are present in the ring of choanocytes comprising the chamber and a small amoeboid cell adjacent to the chamber (open white arrowhead) and an archaeocyte (red arrowhead). An archaeocyte without labelled microbes is marked with a white arrowhead. These three cells are outlined. (**G-I**) Fluorescence micrographs of juveniles at 2 hpe to microbes from healthy (**G**) and unhealthy *A. queenslandica* (**H**), and *R. globostellata* (**I**). Microbes are present in choanocyte chambers and small amoebocytes (open white arrowheads) in all three treatments (see Figs S1 and S2). Scale bars, 25 µm. (**J**) The mean number (± standard error) of total and microbe-containing archaeocytes, and choanocyte chambers in juvenile optical sections from each treatment group (n = 20). Significant differences based in a one-way ANOVA followed by the Tukey's HSD post-hoc test ($p < 0.01$) are denoted an asterisk (*).

Figure 2. Rapid and transient induction of immunity genes by native symbionts. (**A**) PCA of transcriptomes from juvenile *A. queenslandica* exposed to FSW (n = 28; grey; 0 hpe controls, circles); foreign bacteria (n = 8; FB, red); native bacteria from healthy (n = 10; HNB, blue) and unhealthy *A. queenslandica* (n = 10; UNB, cyan) at 2 (triangles) and 8 (squares) hpe. 95% confidence ellipses shown. (**B**) UpSet plot summarising the relationship of significantly differentially expressed coding sequences induced by native and foreign bacteria at 2 and 8 hpe relative to FSW (DESeq2; *p*-adj < 0.05). The number of differentially expressed genes in each bacterial treatment is to the left in bold. The number of differentially expressed coding sequences intersecting between treatment groups at the top of each bar. The colour coding follows (A) except for gene intersecting between healthy and unhealthy native bacterial treatment (teal bars). Grey bars, intersections between native and foreign bacteria. (**C**) Hierarchically clustered heatmap of differentially expressed TF genes (*p*-adj < 0.05). TF

names are shown to the left. (**D**) Slope charts of the variation in the number of the differentially expressed TFs, PRRs (SRCRs, GPCRs, IgSFs) and immunity signalling pathway components (ISPs) induced by bacterial at 2 and 8 hpe. (**E**) Genes encoding conserved enzymes involved in xenobiotic metabolism activated by foreign bacteria, with phases shown to the right. z-score for C and E shown in the middle. (**F**) Network diagram of the top 30 connected co-expressed genes induced by healthy native bacteria based on WGCNA. The degree of connectivity is indicated by the thickness of the edges/connections. The number of edges is represented by the size of the gene nodes. The nodes with black fill indicate genes identified by sPLS-DA as key differentiators between responses to native symbionts versus foreign bacteria (Figure S4 and Table S4). All genes are in WGCNA module 1 (blue), except the TRAF in brown (module 2) (Figure S7 and Tables S6 and S7).

Figure 3. Subcellular localization of IRF, STAT, and NF-κB in response to native and foreign bacteria. (**A-D**) Immunostained 2 hpe juveniles exposed to FSW; (**E-H**) foreign bacteria; and (**I-L**) healthy native bacteria (IRF, NF-κB or STAT, red; foreign or native bacteria, green; nuclei, blue): (**A,E,I**) IRF; (**B,F,J**) NF-κB; and (**C,G,K**) STAT. (**D,H,L**) Diagrams of a choanocyte chamber (Ch) with proximal and two distant amoebocyte cell types (pAm, dAm1 and dAm2) and archeocytes (Ar) showing the nuclear localisation of IRF (green), NF-κB (orange) and STAT (blue) in juveniles reared in FSW (**D**), or exposed to foreign bacteria (**H**) or native bacteria (**L**). IRF localisation in the cytoplasm in distal amoebocytes dAM1 is shown in **H**. Red and blue speckled colouring demarcates the cells housing foreign and native bacteria at 2 hpe, respectively. Arrows and question marks indicate the unknown lineage relationship between amoebocytes to each other and to archaeoctyes, including transdifferentiation (Sogabe et al. 2019). Scale bars, 10 µm.

Figure 1

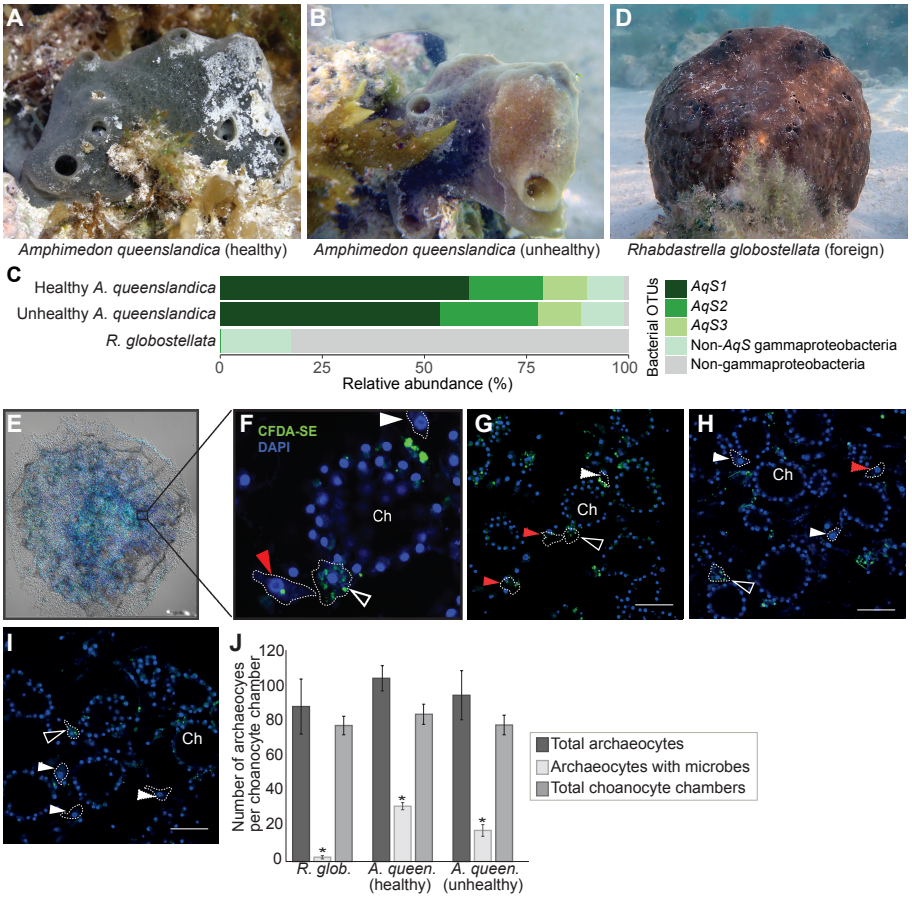
A
B
D
Amphimedon queenslandica (healthy)
Amphimedon queenslandica (unhealthy)
Rhabdastrella globostellata (foreign)
C
Healthy A. queenslandica
Unhealthy A. queenslandica
R. globostellata
0
25
50
75
100
Relative abundance (%)
Bacterial OTUs
AqS1
AqS2
AqS3
Non-AqS gammaproteobacteria
Non-gammaproteobacteria
E
F
CFDA-SE
DAPI
Ch
G
Ch
H
Ch
I
Ch
J
Number of archaeocyes per choanocyte chamber
120
100
80
60
40
20
0
R. glob.
A. queen. (healthy)
A. queen. (unhealthy)
Total archaeocytes
Archaeocytes with microbes
Total choanocyte chambers

Figure 2

A
Unhealthy native bacteria (UNB)
Healthy native bacteria (HNB)
Foreign bacteria (FB)
FSW
PC2
PC1
0 hpe
2 hpe
8 hpe
B
Number of genes intersecting
HNB 2 hpe 1872
HNB 8 hpe 384
UNB 2 hpe 1219
UNB 8 hpe 1250
FB 2 hpe 721
FB 8 hpe 950
C
FSW FB HNB UNB FSW FB HNB UNB
2 hpe 8 hpe
D
TFs
SRCRs
GPCRs
IgSFs
ISPs
PRRs
Number of genes
hpe
Conserved immunity TFs
bZIP
ETS
C2H2-ZnF
Fox
E
Antioxidant
Antioxidant mediator
Hydrolysis
Phase I oxidation
Phase I reduction
Phase II conjugation
Phase III transport
Protea-somal degradation
Z-score
F
Dredd
WWP1
TAB1
HIPK1
PIAS1
BCL2
IgTIR1
PDCD10
SDCBP
slmb
ERBB4
TNF-AIP8
BCL3
IRF
TRAF3
JAK2
CEB-PBβ
STAT
CUL1
BCL2-L2
TRAF
MYD88
CEBPBb
MALT1
TRAF3IP1
IRF2BP2
NF-κB
TRAF
Eff
TGF-β

Figure 3

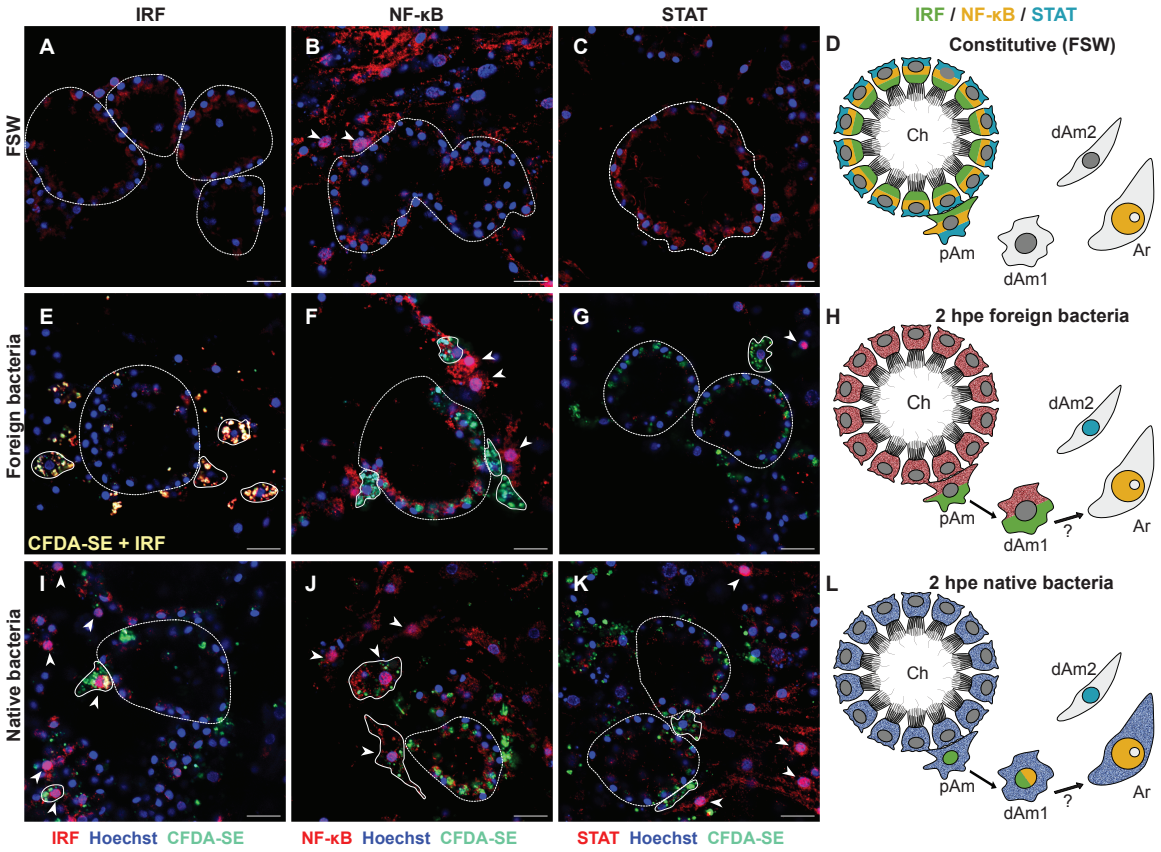
IRF
NF-κB
STAT
IRF / NF-κB / STAT
FSW
Foreign bacteria
Native bacteria
A
B
C
D
Constitutive (FSW)
Ch
dAm2
pAm
dAm1
Ar
E
F
G
H
2 hpe foreign bacteria
CFDA-SE + IRF
?
I
J
K
L
2 hpe native bacteria
IRF Hoechst CFDA-SE
NF-κB Hoechst CFDA-SE
STAT Hoechst CFDA-SE